Journal of Molecular Structure 1084 (2015) 274–283

Contents lists available at ScienceDirect

Journal of Molecular Structure

journal homepage: www.elsevier.com/locate/molstruc

Structural elucidation, density functional calculations and contribution of intermolecular interactions in cholest-4-en-3-one crystals: Insights from X-ray and Hirshfeld surface analysis

Hena Khanam [a], Ashraf Mashrai [a], Nazish Siddiqui [b], Musheer Ahmad [c], Mohammad Jane Alam [d], Shabbir Ahmad [d], Shamsuzzaman [a,*]

[a] Steroid Research Laboratory, Department of Chemistry, Aligarh Muslim University, Aligarh 202002, UP, India
[b] Department of Ilmuladvia, Aligarh Muslim University, Aligarh 202002, India
[c] Department of Chemistry, Indian Institute of Technology, Kanpur 208016, India
[d] Department of Physics, Aligarh Muslim University, Aligarh 202002, India

HIGHLIGHTS

- Synthesis and single crystal structure of cholest-4-en-3-one has been performed.
- Hirshfeld surface analysis has been used for the identification of intermolecular contacts.
- The theoretical study was attempted to predict the optimized geometry by DFT.
- Optical, morphological, and microstructral properties has also been explored.

GRAPHICAL ABSTRACT

In the present work we have described synthesis and single crystal X-ray analysis of cholest-4-en-3-one. Intermolecular interactions have been studied through Hirshfeld surface analysis/finger print plot. In addition density functional calculations have also been performed.

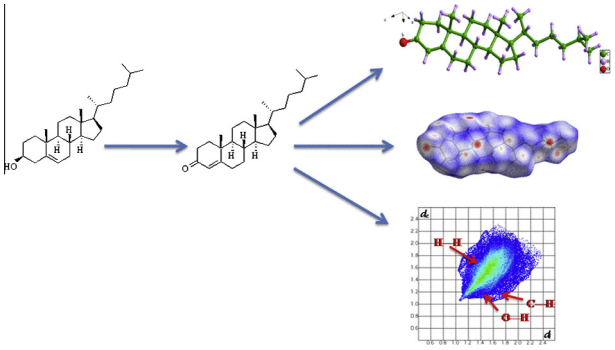

ARTICLE INFO

Article history:
Received 3 September 2014
Received in revised form 5 December 2014
Accepted 8 December 2014
Available online 19 December 2014

Keywords:
Steroids
Cholest-4-en-3-one
X-ray
Hirshfeld
DFT

ABSTRACT

The foremost objective of the present work is systematic analysis of intermolecular interactions in crystal structure of cholest-4-en-3-one (**2**) molecule. It is accomplished by Hirshfeld surface analysis and finger-print plot. Hirshfeld surface analysis has been used to visualize the fidelity of the crystal structure. This method permitted for the identification of individual types of intermolecular contacts and their impact on the complete packing. Molecules are linked by a combination of C═O—H, C—H—H, and C—H contacts, which have clear signatures in the fingerprint plots. The theoretical study was attempted to predict the optimized geometry and computed spectra by the Density Functional Theory (DFT) using the B3LYP function with the 6–311++G(d,p) basis set. Atomic charges, MEP mapping, HOMO–LUMO, various thermodynamic and molecular properties have been reported. In addition thermal stability, optical, morphological, and microstructral properties of the title compound (**2**) have also been explored.

* Corresponding author. Tel.: +91 9411003465.
E-mail address: shamsuzzaman9@gmail.com (Shamsuzzaman).

http://dx.doi.org/10.1016/j.molstruc.2014.12.027
0022-2860/

Introduction

The chemistry of steroids is of significant importance because of the roles undertaken by these molecules in both animals and plants [1]. An attractive feature of steroidal structures would be their applications in crystal engineering, which would take advantage of their tendency to occur in different crystal forms [2]. The interesting structural and stereochemical features of the steroid nucleus provide additional fascination to the researchers, and thereby alterations in the steroidal skeleton have been envisaged to discover new chemical entities with a potential to afford some promising drugs of the future [3]. During the second half of the last century, chemical studies on steroids, including cholesterol, were intensively conducted. Cholesterol, as an allylic alcohol with a large hydrophobic portion, undergoes various transformations and can be applied in various chemical syntheses, such as steroid hormones, ecdysteroids, vitamin D derivatives and brassinosteroids. Cholesterol is frequently used as a model system for testing many constructive chemical and enzymatic reactions, which have been now widely used for multi-step steroid transformations leading to products of practical importance. Cholest-4-en-3-one, a cholesterol derivative, is an important synthetic intermediate in many steroid transformations [4]. It has been shown to be implicated in the metabolic pathways from cholesterol to 5α-cholest-7-en-3β-ol and 5β-cholestanol [5]. From the structural point of view, cholest-4-en-3-one crystals have a monoclinic structure with a space group $P2_1$ with cell parameters a = 14.634 (5), b = 7.862 (5), c = 10.674 (5) Å, β = 105.1 (2)°, Z = 2 [6]. There has been observed the growing interest in applications of Hirshfeld surface analysis in the field of crystallography, as this approach is a very convenient tool for the investigation of different kinds of intermolecular interactions. Since crystal structure gives the most definite understanding of the intermolecular contacts and crystal packing, Hirshfeld surface [7–9] based tools appear to be particularly suitable for the visualization of variations in the intermolecular interactions of the compounds. The surfaces encode information about all intermolecular interactions offer a facile way for obtaining an idea on crystal packing. The breakdown of the associated fingerprint plots [10] explores quantitatively the types of intermolecular contacts experienced by molecules and presents this information in a convenient color plot. As part of our ongoing studies on synthesis and single crystal X-ray analysis of steroids [11], the single crystal analysis was undertaken along with the Hirshfeld surface analysis to investigate the close contacts. Theoretical calculations were performed by using B3LYP function with the 6–311++G(d,p) basis set. Besides, spectral, thermal, optical and morphological properties were also investigated.

Experimental

General comments

All reagents and solvents were commercially available and used as received. Melting point was determined on digital auto melting point apparatus. Elemental analysis of the compound was recorded on Perkin Elmer 2400 CHN Elemental Analyzer. The IR spectrum was recorded on KBr pellets with Spectrum Two by Perkin Elmer Spectrometer and values are given in cm^{-1}. ^1H and ^{13}C NMR spectra were run in $CDCl_3$ on a Bruker Avance II 400 NMR Spectrometer at 400 MHz and 100 MHz respectively. Chemical shifts (δ) are reported in ppm relative to the TMS (^1H NMR, 400 MHz) and to the solvent signal (^{13}C NMR spectra, 100 MHz) and coupling constants are given in Hz. Thermal study of the compound was carried out using TGA/DTA- 60H instrument (SHIMADZU) at a heating rate of 20 °C min^{-1} from ambient temperature to 800 °C. Powder X-ray diffraction (Cu Kα radiation, scan rate 3°/min, 293 K, λ = 1.54 Å) was performed on a Bruker D8 Advance Series 2 powder X-ray diffractometer. UV–visible spectrum was recorded on UV–vis spectrophotometer (Perkin Elmer Life and Analytical Sciences, CT, USA) in the wavelength range of A 200–700 nm. The fluorescence spectrum was collected at 37 °C with a 1 cm path length cell using a Hitachi spectrofluorometer (Model 2500) equipped with a PC and the emission slit were set at 5 nm. The emission spectrum was recorded in the range of 300–800 nm. The surface morphology of the compound was monitored using JEOL JSM-6510LV scanning electron microscope (SEM), equipped with energy-dispersive X-ray spectroscopy (EDX) analyzer.

Synthesis of cholest-4-en-3-one

Synthesis of the title compound (**2**) (m.p. 80–81 °C) was performed by reported method [12]. Recrystallization from methanol afforded cholest-4-en-3-one crystals as colorless needles suitable for X-ray diffraction (Scheme 1).

Anal. Calcd for $C_{27}H_{44}O$: C, 84.31; H, 11.53. Found: C, 84.48; H, 11.38; IR (KBr, cm^{-1}): 2943, 2866 (C—H, stretching), 1673 (C=O), 1617 (C=C); ^1H NMR ($CDCl_3$, 400 MHz): δ ppm: 5.72 (1H, s, C4—H), 1.18 (3H, s, 10-CH_3) 0.71 (3H, s, 13-CH_3), 0.92 & 0.85 (other methyl protons); ^{13}C NMR ($CDCl_3$, 100 MHz): δ ppm: 199.6, 171.7, 123.7, 56.1, 55.8, 53.8, 42.3, 39.6, 39.5, 38.6, 36.1, 35.7, 35.6, 35.6, 33.9, 32.9, 32.0, 28.1, 28.0, 24.1, 23.8, 22.8, 22.5, 21.0, 18.6, 17.3, 11.9. MS(EI): m/z 384.34 [M^+].

X-ray crystallographic study

Single crystal X-ray data of compound **2** was collected at 100 K on a Bruker SMART APEX CCD diffractometer using graphite monochromated Mo K_α radiation (λ = 0.71073 Å). The linear absorption coefficients, scattering factors for the atoms, and the anomalous dispersion corrections were taken from the International Tables for X-ray Crystallography [13]. The data integration and reduction were carried out with SAINT [14] software. Empirical absorption correction was applied to the collected reflections with SADABS [15] and the space group was determined using XPREP [16]. The structure was solved by the direct methods using SHELXTL-97 [17] and refined on F^2 by full-matrix least-squares using the SHELXL-97 [18] program package. All non-hydrogen atoms were refined anisotropically. Crystallographic data (excluding structure factors) for the structures reported in this article have been deposited with the Cambridge Crystallographic Data Centre (CCDC) as deposition no. CCDC 99399. All H-atom positions were calculated geometrically with U_{iso} (H) = 1.2–1.5 Å U_{eq} (parent atom). A riding model was used in their refinement (C—H=0.98–1.00 Å).

Hirshfeld surfaces calculations

Molecular Hirshfeld surfaces [7] in the crystal structure have been constructed based on the electron distribution calculated as the sum of spherical atom electron densities [19]. For a given crystal structure and set of spherical atomic electron densities, the Hirshfeld surface is unique [20], and it is this property that suggests the possibility of gaining additional imminent into the intermolecular interaction of molecular crystals. The Hirshfeld surfaces and fingerprint plots presented here were generated using CrystalExplorer [21] based on results of X-ray studies. During the calculations, bond lengths to hydrogen atoms were normalized to standard neutron values (C—H=1.083 Å) [22] in order to ensure the internal consistency and independence of results from the crystal structure refinement method. The 2D fingerprint plots displayed by using the standard 0.6–2.6 Å view with the d_e and d_i distance scales displayed on the graph axes. The normalized contact

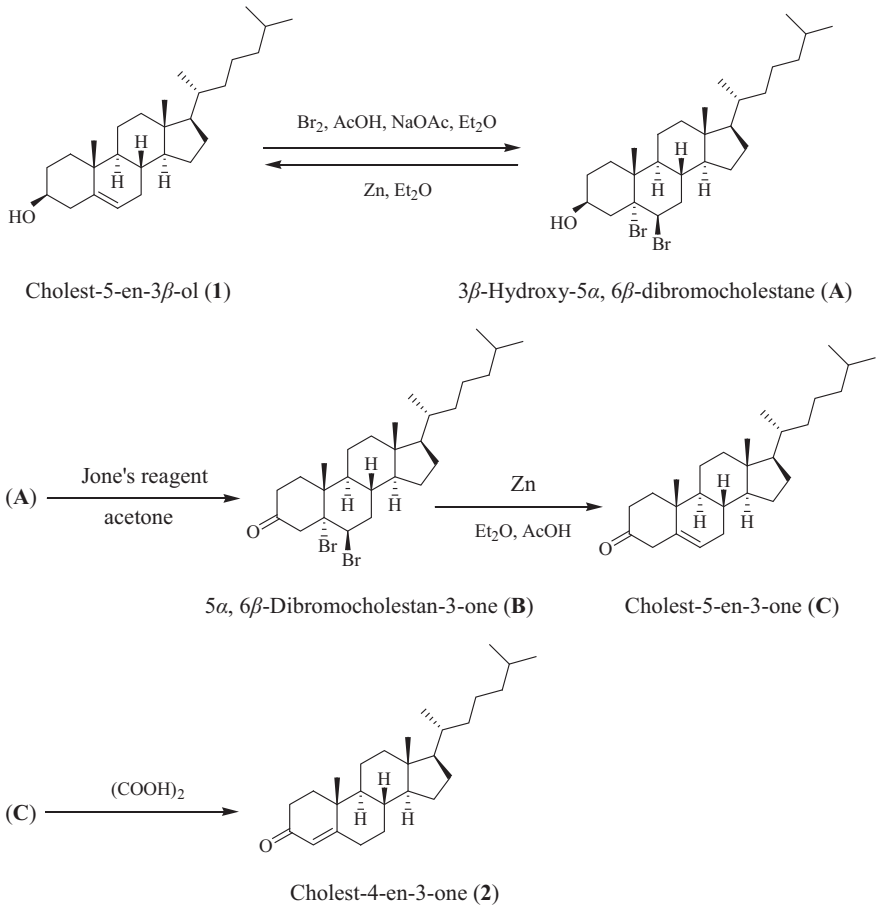

Scheme 1. Synthesis of cholest-4-en-3-one.

distance (d_{norm}) based on both d_e, d_i and the *vdw* radii of the atom, given by Eq. (1) enables identification of the regions of particular importance to intermolecular interactions [7]. Because of the symmetry between d_e and d_i in the expression for d_{norm}, where two Hirshfeld surfaces touch, both will display a red spot identical in color intensity as well as size and shape.

$$d_{norm} = \frac{d_i - r_i^{vdw}}{r_i^{vdw}} + \frac{d_e - r_e^{vdw}}{r_e^{vdw}} \quad (1)$$

Theoretical calculations

The entire theoretical calculations were performed at Density Functional Theory using Gaussian 03W [23] The molecular geometry and vibrational spectra of the present molecule have been computed using DFT (B3LYP) method with 6–311++G(d,p) basis set.

Results and discussion

IR, ^{1}H NMR, ^{13}C NMR, elemental analysis and single crystal XRD data are compatible with the putative structure depicted in Scheme 1.

Description of crystal structure

The title compound (**2**) crystallizes in the monoclinic system, space group $P2_1$ which can be explained by the presence of 7 *chiral* centers [22]. There is only one molecule in the asymmetric unit, while unit cell contains 2 molecules. The molecules are arranged in head to tail manner and the crystal packing is stabilized by a combination of intermolecular interactions (C═O—H, C—H—H, C—H) (Figs. 1–3). Rings B and C exist in normal chair conformation. Ring A adopts sofa conformation (because of the presence of double bond), and ring D is intermediate between envelope & half-chair. The A/B ring junction is *quasi-trans*, while the B/C and C/D ring systems are *trans* fused about the C(8)—C(9) and C(14)—C(15) bonds, respectively. The bond distances and bond angles in compound **2** are found to be almost equivalent to reported earlier [6], Ring bond lengths have normal values with an average of 1.528 (3) Å, while the cholestane side chain shows an average bond length of 1.521 (3) Å. The bond length C(1)—O and C(6)—C(5) are 1.224 (3) and 1.340 (4) Å respectively, which indicates a double-bond character [24]. Side-chain is fully extended with a *gauche-trans* conformation of the terminal C27 and C28 methyl groups. The absolute configurations of *chiral* centers were determined from the structure presented, these sites exhibit the following chiralities: C4 = *R*, C8 = *S*, C9 = *S*, C14 = *R*, C15 = *S*, C17 = *R* and C20 = *R*. Since there is no strong hydrogen bond donor in the molecule, cohesion of the crystal structure can only be attributed to van der Waals interactions. Pertinent crystallographic data and refinement details for the structural analyses of the compound **2** are summarized in Tables 1 and 2. It is important to note that earlier report [6] did not provide any information regarding the presence of intermolecular contacts, but we have explored and studied deeply the presence of short intermolecular contacts and this has been well analyzed by Molecular Hirshfeld surfaces.

Molecular Hirshfeld surfaces

Hirshfeld surface is a useful tool for describing the surface characteristics of the molecules. It represents the area where molecules

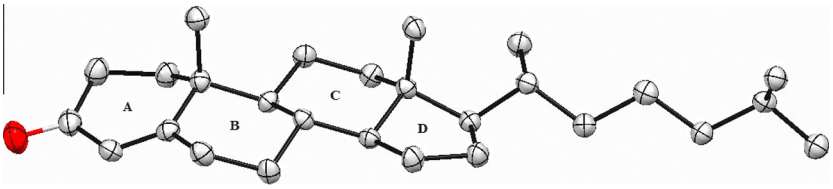

Fig. 1. ORTEP view of cholest-4-en-3-one, ellipsoids are drawn at 50% probability level.

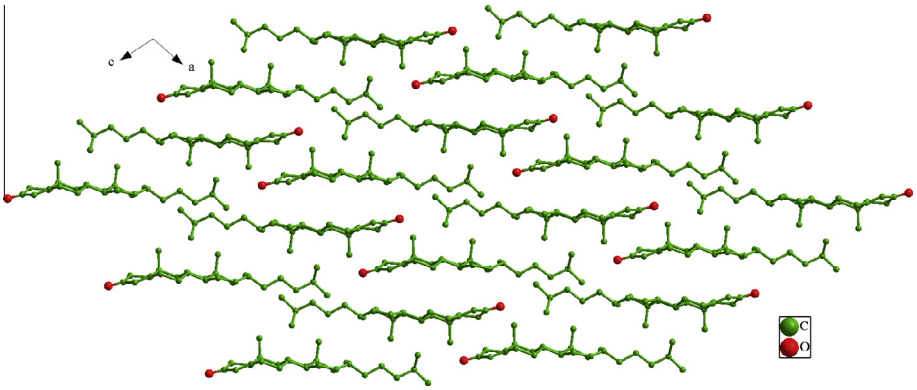

Fig. 2. 2D-view of cholest-4-en-3-one.

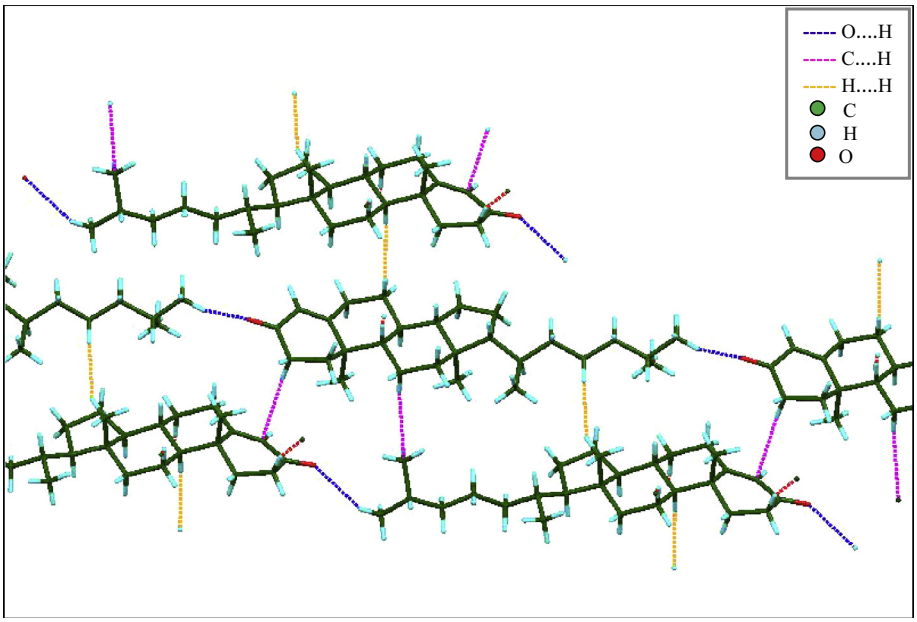

Fig. 3. Short intermolecular contacts present within the cholest-4-en-3-one molecules.

come into contact, therefore, its analysis gives the possibility of obtaining additional insight into the intermolecular interactions in the crystal state. The Hirshfeld surface enclosing a molecule is defined by points where the contribution to the electron density from the molecule of interest is equal to the contribution from all the other molecules. For each point on that isosurface two distances are defined: d_e (the distance from the point to the nearest nucleus external to the surface), and d_i (the distance to the nearest nucleus internal to the surface). The molecular Hirshfeld surfaces of cholest-4-en-3-one were generated using a standard (high) surface resolution with the 3D d_{norm} surfaces were mapped over a fixed color scale of −0.23 (red) to 1.2 Å (blue), the shape index mapped in the color range of −0.99 to 1 and curvedness in the range of −4.0 to 0.4. The molecular Hirshfeld surface (d_{norm}, shape index and curvedness) of cholest-4-en-3-one are shown in Fig. 4a–c. For comparison of intermolecular interactions scheme in crystal structures, the normalized contact distances, d_{norm}, based on van der Waals radii, were mapped into the Hirshfeld surfaces. In the color scale, negative values of d_{norm} are visualized by the red color, indicating contacts shorter than the sum of van der Waals radii. The white color denotes intermolecular distances close to van der Waals contacts with d_{norm} equal to zero. In turn, contacts longer than the sum of van der Waals radii with positive d_{norm} values are indicated by blue. The O—H and C—H interaction in compound **2** can be seen in the Hirshfeld surface as the bright red areas. The other visible spots on the surface correspond to H—H contacts

Table 1
Crystal data and structure refinement for cholest-4-en-3-one.

Empirical formula	$C_{27}H_{44}O$
Formula mass	384.62
Wavelength (λ)	0.71073 Å
Crystal system	Monoclinic
Space group	$P2_1$
Unit cell dimensions	
a, Å	10.543(5)
b, Å	7.786(5)
c, Å	14.506(5)
α (°)	90.000
β (°)	105.919(5)
γ (°)	90.000
Volume, Å^3	1145.1(10)
No. of molecules per unit cell (Z)	2
Calculated density, Mg m^{-3}	1.116
Absorption coefficient (μ, mm^{-1})	0.065
F(000)	428
Crystal size	0.21 × 0.14 × 0.10 mm
θ range for data collection	1.46–25.50°
Limiting indices	$-11 \leqslant h \leqslant 12$, $-9 \leqslant k \leqslant 9$, $-15 \leqslant l \leqslant 17$
Goodness-of-fit on F^2	1.067
Final R indices [$I > 2\sigma(I)$]	$R1$ = 0.0525, w$R2$ = 0.1194
R indices (all data)	$R1$ = 0.0674, w$R2$ = 0.1384

$R_1 = \Sigma||F_o| - |F_c||/\Sigma|F_o|$ with $F_o^2 > 2\sigma(F_o^2)$. $wR_2 = [\Sigma w(|F_o^2|-|F_c^2|)^2/\Sigma|F_o^2|^2]^{1/2}$.

(Fig. 4a). Shape index (Fig. 4b) is a measure of "which shape", and it can be sensitive to very subtle changes in surface shape, particularly in areas where the total curvature (or the curvedness) is very low. The information conveyed by shape index is consisted with the 2D fingerprint plot. The curvedness (Fig. 4c) is the measurement of "how much shape"; the flat areas of the surface correspond to low values of curvedness, while sharp curvature areas correspond to high values of curvedness and usually tend to divide the surface into patches, indicating interactions between neighboring molecules. The 2D fingerprint plots can be decomposed to highlight particular atom pair close contacts [19]. This decomposition enables separation of contributions from different interaction types, which overlap in the full fingerprint. The 2D fingerprint plots, which analyses all of the intermolecular contacts at the same time, revealed that the main intermolecular interactions in compound were C—H, C—H—H, and C=O—H intermolecular interactions (Fig. 5a). C=H—H interactions, which were reflected in the middle of scattered points and cover most area in the 2D fingerprint plots, have a most significant contribution to the total Hirshfeld surfaces (88.5%) (Fig. 5b). The O—H/H—O contacts appear as distinct spikes pointing toward the lower left of the plot (Fig. 5c). Complementary regions are visible in the fingerprint plots where one molecule act as donor ($d_e > d_i$) and the other as an acceptor ($d_e < d_i$). The shortest contact i.e., the minimum value of ($d_e + d_i$) is around 1.9 Å point out the importance of these interactions. The proportion of O—H/H—O interactions comprising 8.8% of the total Hirshfeld surfaces for each molecule of (**2**). At the top left and bottom right of the fingerprint plot, there are characteristic

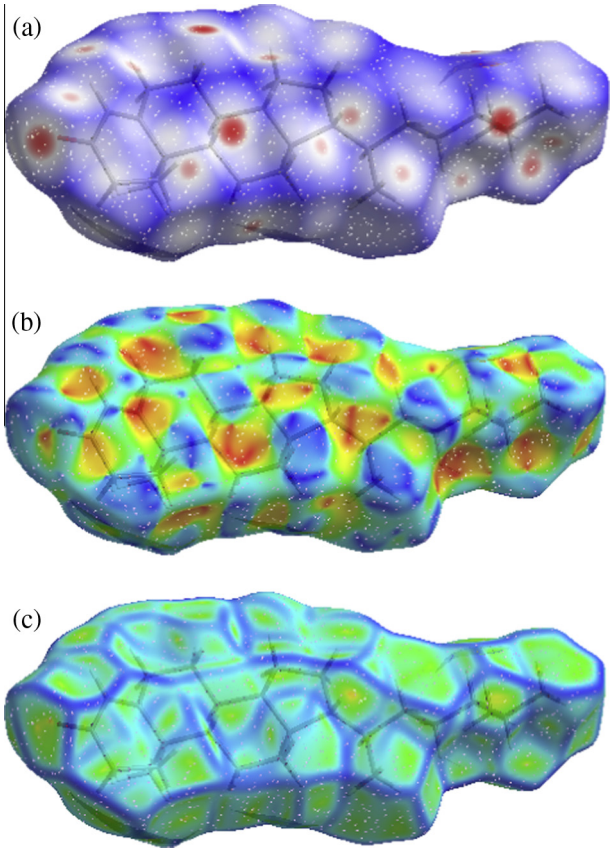

Fig. 4. Hirshfeld surfaces mapped with (a) d_{norm}, (b) *surface index* and (c) *curvedness* of cholest-4-en-3-one. The surfaces are shown as transparent to allow visualization of the orientation and conformation of the functional groups in the molecules.

"wings" which are identified as a result of C—H interactions (Fig. 5d). The decomposition of the fingerprint plot shows that C—H/H—C contacts comprise 2.8% of the total Hirshfeld surface area. Fig. 6 contains the percentages of contributions for a variety of contacts in the title crystal structure. Thus the nature of the interplay of the title compound is more easily understood using Hirshfeld surface, with the results further highlighting the power of the technique in mapping out the interactions within the crystal and this methodology has very important promise in crystal engineering. Undoubtedly, the Hirshfeld surface allows a much more detailed scrutiny by displaying all the intermolecular interactions and by quantifying them in 2D fingerprint plot within the crystal. In fact it is a novel tool in crystal structure prediction.

Theoretical study

Frontier molecular orbitals

The frontier orbitals, HOMO and LUMO are imperative parameters for determining the way the molecules interacts with other

Table 2
Optimized structural parameters (selected bond lengths and bond angles) of cholest-4-en-3-one at B3LYP/6–311++G(d,p) level of theory.

Bond lengths (Å)			Bond angles (°)		
	Experimental[a]	Calculated (B3LYP/6–311G(d,p))		Experimental[a]	Calculated (B3LYP/6–311G(d,p))
C1—O1	1.224(3)	1.223	C2C1O1	121.6(3)	122.38
C2—C1	1.491(4)	1.519	C6C1O1	121.7(3)	121.90
C1—C6	1.466(4)	1.472	C1C6C5	123.8(3)	124.38
C6—C5	1.340(4)	1.349	H6C6C5	121(2)	120.43
C5—C11	1.496(4)	1.509	C4C5C11	116.7(2)	116.87

[a] Obtained from single crystal XRD data.

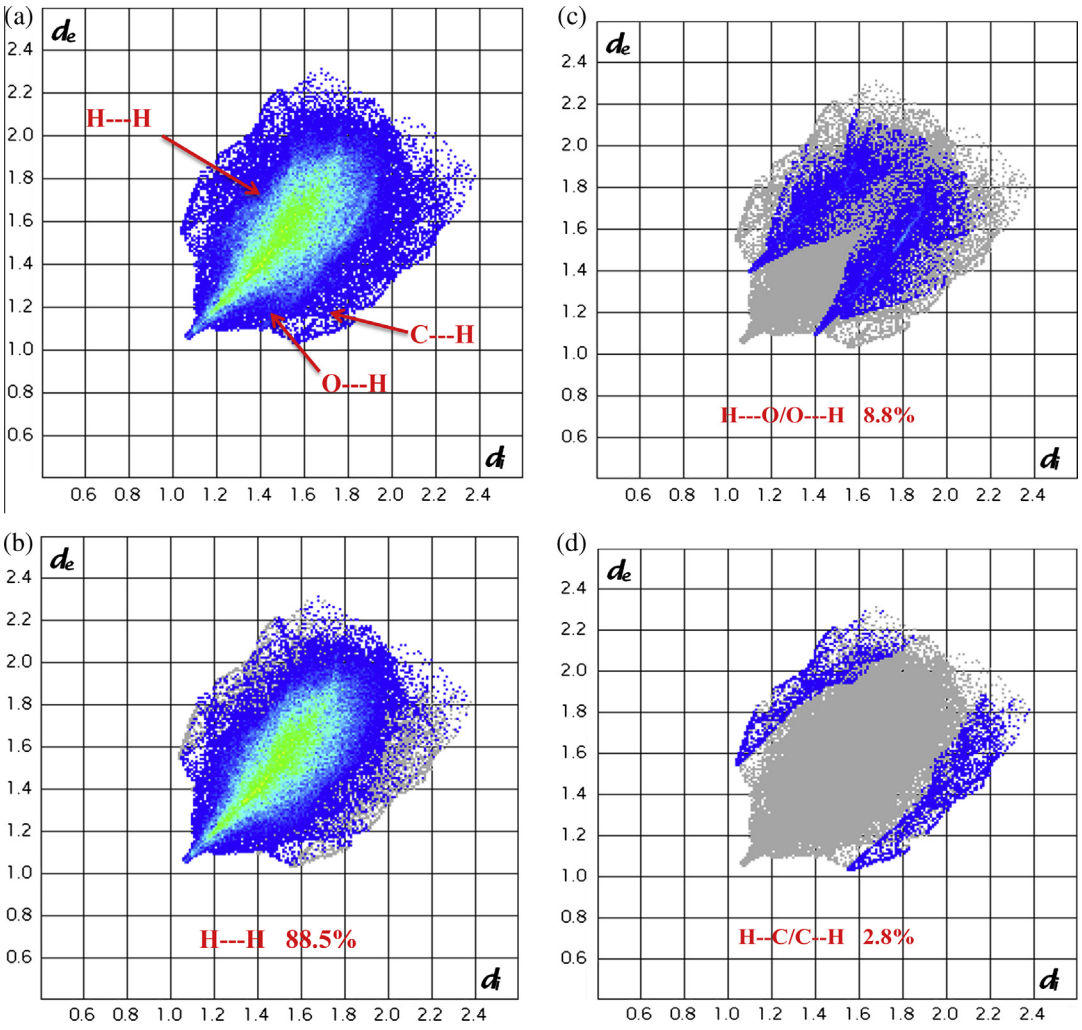

Fig. 5. 2D fingerprint plots of cholest-4-en-3-one: (a) full (b) resolved into H—H and (c) O—H (d) C—H contacts showing the percentages of contacts contributed to the total Hirshfeld surface area of molecule.

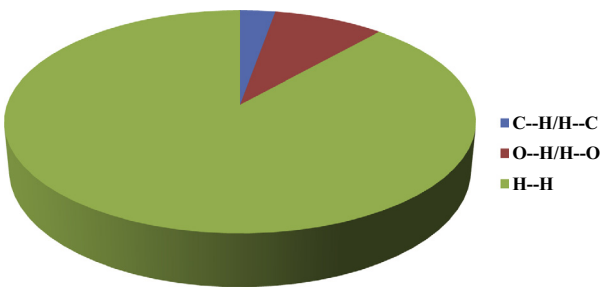

Fig. 6. Relative contribution of various intermolecular interactions to the Hirshfeld surface area.

species (Fig. 7). HOMO, the outermost orbital containing electrons has tendency to release electrons as an electron donor. On the other hand; LUMO orbital has free space to accept electrons as electron acceptor. The ability of charge transfer interactions within molecule can be explained by the HOMO–LUMO energy gap. The positive and negative phases are represented by red and green color, respectively. The energy values correspond to HOMO and LUMO and their energy gap show the chemical activity and kinetic stability of the molecule. The HOMO–LUMO energy and the gap between them, at B3LYP/6–311++G(d,p), are given as follows:

HOMO energy = −6.2 eV.
LUMO energy = −1.13 eV.
HOMO–LUMO energy gap = −5.07 eV.

The lowering of HOMO–LUMO energy gap supports bioactive property of the molecule. Gauss-Sum 2.2 program [25] was used to create the density of states spectrum (DOS) by convoluting the molecular orbital information with Gaussian curves of unit height (Fig. S1). The green and blue lines in the DOS spectrum indicated the HOMO and LUMO levels.

Molecular electrostatic potential map

The molecular electrostatic potential (MEP) maps have been used to predict the behavior and reactivity of the molecules. It is mapping potentials created in the space around a molecule by its nuclei and electrons. MEP map is very constructive for the qualitative interpretation of the electrophilic and nucleophilic reactions for the study of biological recognition process and hydrogen bonding interactions [26]. This also provides information for understanding the shape, size, charge density, delocalization and site of chemical reactivity of the molecules. There are three important colors; blue, red and green used to indicate the value of the electrostatic potential. The surfaces with blue and red colors show the positive and negative values of the potential respectively. The surfaces with green colors indicate zero potential. MEP map for the

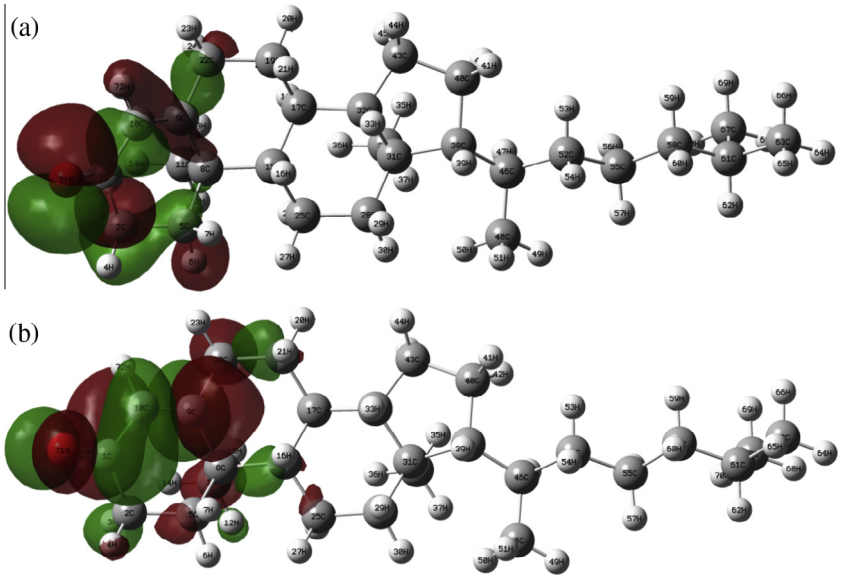

Fig. 7. Cholest-4-en-3-one (a) HOMO (b) LUMO.

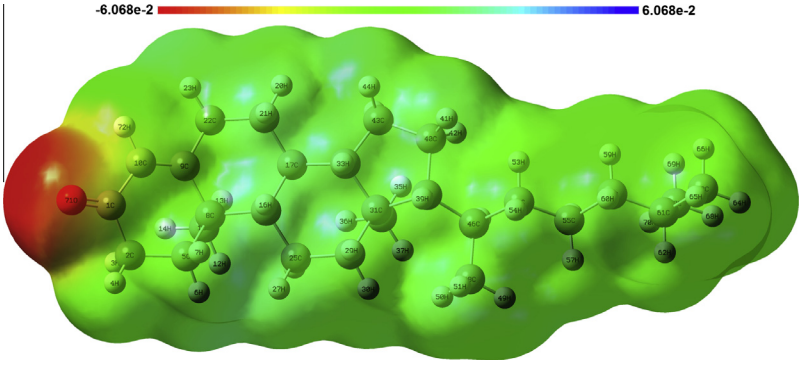

Fig. 8. MEP map for cholest-4-en-3-one.

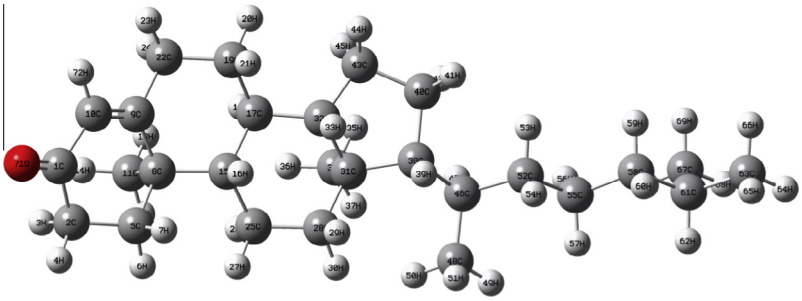

Fig. 9. The optimized molecular structure of cholest-4-en-3-one.

cholest-4-en-3-one at B3LYP/6–311G(d,p) level of theory is shown in Fig. 8 with color[1] range from $-6.068e^{-2}$ (deepest red) to $+6.068e^{-2}$ (deepest blue). The red color surfaces with negative MEP belong to high electron density, indicating a strong attraction between the proton and points on the molecular surface. The blue color surfaces correspond to areas of lowest electron density (Table S1).

Molecular geometry

The optimized molecular structure of cholest-4-en-3-one along with numbering of atoms is shown in Fig. 9. For the optimized geometry, the minimum energy value was found as −1130.6821 a.u. In the present work, the calculated optimized geometrical parameters are found in a reasonable agreement with the X-ray diffraction data (Table 2).

Vibrational analysis

Cholest-4-en-3-one is a *chiral* molecule and belongs to C1 point group. The theoretical wave numbers corresponding to these bands

[1] For interpretation of color in Fig. 8, the reader is referred to the web version of this article.

Table 3
Theoretical computed zero point vibrational energy (kcal mol^{-1}), rotational constants (GHz), rotational temperature (K), thermal energy (kcal mol^{-1}), molar capacity at constant volume and entropy (cal mol^{-1} K^{-1}) at STP.

Parameters	B3LYP/6–311++G(d,p)
Zero point vibrational energy	415.78342
Rotational constants	0.58816
	0.05315
	0.05158
Rotational temperatures	0.02823
	0.00255
	0.00248
Energy total	433.967
Translational	0.889
Rotational	0.889
Vibrational	432.189
Molar capacity at constant volume	
Total	116.246
Translational	2.981
Rotational	2.981
Vibrational	110.285
Entropy total	187.497
Translational	43.731
Rotational	36.542
Vibrational	107.223

were found to be in good agreement with the experimental values (Fig. S2).

Other molecular properties

The dipole moment and polarizability tensor are important molecular properties for providing information about a distribution of charge within a molecule. The isotropic polarizability is a measure of electronic distribution in a molecule, caused by an external electric field. The permanent electric dipole moment of a molecule is an important indicator of its behavior in physical, chemical and biological process [27]. It is measure of the charge density in a molecule and is a reactivity index which is important to define biological properties related to the interaction with active site of an enzyme [28]. The magnitude and direction of dipole moment are sensitive to molecular size and shape and they serve as tool in conformational analysis [29]. Knowledge on thermodynamic properties is a key in understanding the rate and selectivity of chemical process including design of viable industrial chemical process. Computational methods are valuable and sometimes indispensable tool in obtaining the thermodynamic quantities of molecules. These data not only reflect the extent of intermolecular interactions but they also dictate the character of interaction of biomolecules. Several thermodynamic parameters have been computed at B3LYP method utilizing 6–311++G(d,p) basis set. These are tabulated in Table 3. Calculated electric dipole moments, polarizabilities anisotropy, and hyperpolarizibility value of cholest-4-en-3-one molecule are given in Supplementary Tables S2–S4.

Morphology

It is useful to know the relation between morphological variations and the growth parameters which extends to applied fields including pharmaceuticals, quality control of optoelectronic crystals and industrial crystallization. The morphology of cholest-4-en-3-one crystal was predicted using WinXMorph program [30,31] and it is depicted in Fig. 10. The morphology of cholest-4-en-3-one revealed the well developed four facets such as $(1\,2\,3)$, $(0\,1\,0)$, $(0\,\bar{1}\,\bar{1})$, $(\bar{1}\,\bar{1}\,1)$. The morphology of the grown crystal shows that, $(0\,\bar{1}\,\bar{1})$ facet has larger surface area than other facets. The angle between the facets $(1\,2\,3)$ – $(\bar{1}\,\bar{1}\,1)$, $(\bar{1}\,\bar{1}\,1)$ – $(0\,\bar{1}\,\bar{1})$ and $(0\,\bar{1}\,\bar{1})$ – $(0\,1\,0)$ of grown crystal found from morphology are 120.97°, 56.95° and 150.83° respectively.

FT-IR spectral analysis

Infrared spectroscopy is used to identify the functional groups and modes of vibration of the synthesized compound. A sharp strong band, characteristic of alpha, beta unsaturated carbonyl group (C=O) was found at 1674 cm^{-1}. The characteristic bands in the range of 2869–2945 cm^{-1} were ascribed to C—H stretching vibrations while the band at 1613 cm^{-1} can be assigned to C=C vibrations (Fig. S2a).

NMR analysis

NMR spectroscopy plays a vital role in the structural confirmation of the grown material. ^{1}H NMR spectrum (Fig. S3) of title compound showed a singlet at δ 5.72, attributed to olefinic proton. Angular and side-chain methyl protons were observed at 1.18 (C10—CH_3), 0.71 (C13—CH_3), 0.92 and 0.85 for other methyl

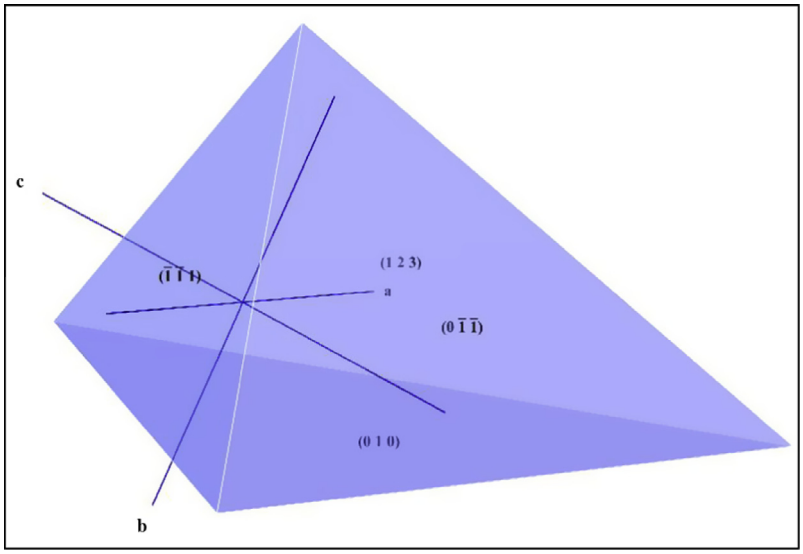

Fig. 10. Equilibrium morphology of cholest-4-en-3-one single crystal.

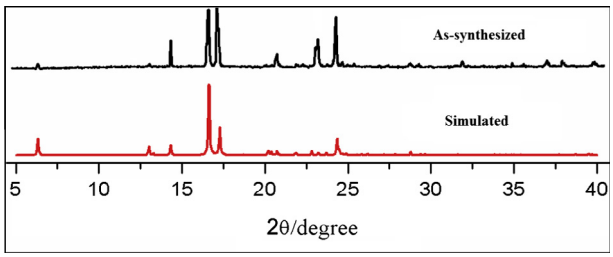

Fig. 11. Powder XRD plots: simulated from CIF and as-synthesised cholest-4-en-3-one.

protons. The characteristic signals in ^{13}C NMR spectrum (Fig. S4) were obtained at δ 199.6 (C=O), 171.7 (C5) and 123.7 (C4). Remaining carbon atoms were seen in accordance to the cholestane series.

Phase identification X-ray powder diffraction (PXRD)

The powder form of the grown crystal (**2**) was subjected to powder X-ray diffraction analysis. The appearance of sharp and strong peaks suggested the good crystallinity of the title compound. The diffractograms of compound are depicted in Fig. 11 which show lower and upper limit of (2θ) between 5.00° and 40.00°. The XRD profile shows that the compound was of single phase without detectable impurity. The lattice parameters of compound were calculated using the powder XRD data and were found in good agreement with the values obtained from single crystals.

Thermal analysis (TG/DTA)

Thermogravimetric/differential thermal analysis (TG/DTA) measurements were performed under nitrogen atmosphere to examine the thermal stabilities of the crystalline sample (compound **2**) and to define the conditions for the thermal treatment on it. The thermograms observed from simultaneous TG/DTA are illustrated in Fig. S5. The TG curve of compound revealed that it is stable up to 240 °C (no weight loss) and does not undergo any phase transition. The TG plot showed two resolved and well-defined decomposition steps. The first decomposition step was found in the temperature range of 240–420 °C with a net weight loss of 92.551% (4.982 mg). The second decomposition step occurred with a temperature range 420–520 °C with a net weight loss of 6.762% (0.364 mg). The disintegration process continued with the confiscation of almost all fragments as gaseous products, leading to the bulk decomposition of the compound before 600 °C since the initial mass of the sample was 5.383 mg and at a temperature of about 600 °C, all the mass was lost and nothing was left as residue. The absence of any weight loss or phase transition around or before its melting point, confirmed the nonexistence of any lattice entrapped solvent or moisture on the grown material. The corresponding DTA curve showed two notable thermal events. The endothermic peaks were obtained at 89 and 354 °C. The sharp endotherm was indicative of a solid-state transition for relatively pure material.

Optical properties (absorption spectra/fluorescence spectra)

UV–visible spectroscopy is one of the best techniques to check the suitability of the grown crystals for optical device fabrications. The UV–visible absorption properties of cholest-4-en-3-one were recorded in dichloromethane solution with the concentration of 10^{-5} M. The absorption spectrum (Fig. S6) exhibited a strong, featureless absorption band around 260 nm, which can be assigned to an allowed $\pi \rightarrow \pi^*$ transition of C=C—C=O system. Fig. S7 shows fluorescence image of the compound which indicated two broad peaks around 350 and 450 nm with different intensities.

Density measurement

The calculated density of $C_{27}H_{44}O$ was obtained by the ratio of the cell mass to cell volume; the equation used to calculate the density is $\rho_{calc} = MZ/NV$, where M is the chemical formula weight of $C_{27}H_{44}O$, Z is the number of formula units in one cell, N is Avogadro's number and V is the volume of the unit cell. According to the crystallographic data, it is observed that $a = 10.543(5)$ Å, $b = 7.786(5)$ Å, $c = 14.506(5)$ Å, $M = 384.62$, $Z = 2$, and $V = 1145.1(10)$ Å^3. So the calculated density of the $C_{27}H_{44}O$ crystal was found to be 1.116 Mg m^{-3}. The experimental density of the cholest-4-en-3-one crystal was measured using the buoyancy method at room temperature (22 °C) in silicon oil. The experimental density of the as-grown $C_{27}H_{44}O$ crystal at 22 °C was found to be 1.118 ± 0.002 Mg m^{-3}, which is almost equal to the calculated density.

Microstructural studies (SEM/EDX)

The crystal surface/morphology of cholest-4-en-3-one was investigated by SEM. A scanning electron microscope (SEM) produces images of a sample by scanning it with a focused beam of electrons. The electrons interact with electrons in the sample, producing various signals that can be detected and that contain information about the sample's surface topography and composition. The signals derived from electron sample interactions reveal information about the sample including external morphology (texture), the chemical composition, and the crystalline structure and orientation of materials making up the sample. The SEM image (Fig. S8) indicated presence of elongated, brick-shaped and some irregular shaped particles with few microcrystals on it. EDX analysis showed presence of C and O (Fig. S9).

Conclusion

In the present study, we have demonstrated synthesis of cholest-4-en-3-one from cholesterol. Its crystal structure was solved by using single crystal X-ray diffraction data. The crystal phase and purity of the compound was established by X-ray powder diffraction (XRD). Moreover spectral, thermal, optical and morphological properties have also been investigated. The study of the title compound underlines the way in which Hirshfeld surface and fingerprint plot analysis provides rapid insight into the intermolecular interactions, which are crucial in crystal packing. Density Functional Theory (DFT) using the B3LYP function with the 6–311++G(d,p) basis set was applied to the solid state molecular geometry obtained from single crystal X-ray studies. The optimized molecular geometry and computed vibrational spectra were compared with experimental results which showed appreciable agreement. Finally, our study emphasizes the utility of Hirshfeld surfaces and in particular, fingerprint-plot analysis for the "visual screening" and detection of crystal structure features through a "whole structure" view of intermolecular contacts.

Acknowledgments

The authors sincerely thank the chairman, department of chemistry Aligarh Muslim University, Aligarh for providing necessary research facilities.

Appendix A. Supplementary material

Supplementary data associated with this article can be found, in the online version, at http://dx.doi.org/10.1016/j.molstruc.2014.12.027.

Reference

[1] A.T. Hulme, R.W. Lancaster, H.F. Cannon, CrystEngComm 8 (2006) 309–312.
[2] C. Guguta, I. Eeuwijk, J.M.M. Smits, R. de Gelder, Cryst. Growth Des. 8 (2008) 823–831.
[3] R. Bansal, S. Guleria, S. Thota, S.L. Bodhankar, M.R. Patwardhan, C. Zimmer, R.W. Hartmann, A.L. Harvey, Steroids 77 (2012) 621–629.
[4] D.V. Banthorpe, B.V. Charlwood, in: Specialist Periodical Reports, Terpenoids and Steroids, vol. 4, The Chemical Society, London, 1974, pp. 250–300.
[5] L.F. Fieser, M. Fieser, Steroids, Reinhold, New York, 1959 (Chapters 17 and 19).
[6] G.M. Sheldrick, E. Oeser, M.R. Caira, L.R. Nassimbeni, R.A. Pauptit, Acta Cryst. B32 (1976) 1984–1987.
[7] M.A. Spackman, J.J. McKinnon, CrystEngComm 4 (2002) 378–392.
[8] (a) J.J. McKinnon, D. Jayatilaka, M.A. Spackman, Chem. Commun. (2007) 3814–3816;
(b) H.F. Clausen, M.S. Chevallier, M.A. Spackman, B.B. Iversen, New J. Chem. 34 (2010) 193–199.
[9] S.K. Seth, I. Saha, C. Estarellas, A. Frontera, T. Kar, S. Mukhopadhyay, Cryst. Growth Des. 11 (2011) 3250–3265.
[10] (a) A.L. Rohl, M. Moret, W. Kaminsky, K. Claborn, J.J. Mckinnon, B. Kahr, Cryst. Growth Des. 8 (2008) 4517–4525;
(b) A. Parkin, G. Barr, W. Dong, C.J. Gilmore, D. Jayatilaka, J.J. Mckinnon, M.A. Spackman, C.C. Wilson, CrystEngComm 9 (2007) 648–652.
[11] (a) Shamsuzzaman, H. Khanam, A. Mashrai, M. Ahmad, Y.N. Mabkhot, W. Frey, N. Siddiqui, J. Cryst. Growth 384 (2013) 135–143;
(b) Shamsuzzaman, A. Mashrai, H. Khanam, Y.N. Mabkhot, W. Frey, J. Mole. Str. 1063 (2014) 219–225.
[12] (a) L.F. Fieser, J. Am. Chem. Soc. 75 (1953) 5421–5422;
(b) L. Ruzicka, W. Bosshard, W.H. Fischer, H. Wirz, Helv. Chim. Acta 19 (1936) 1147–1153.
[13] C.H. MacGillavry, G.D. Rieck, International Tables for X-Ray Crystallography, vol. III, Kynoch Press, Birmingham, London, 1962.
[14] SAINT, Version 6.02; Bruker AXS, Madison, WI, 1999.
[15] G.M. Sheldrick, SADABS: Empirical Absorption Correction Program, University of Göttingen, Göttingen, Germany, 1997.
[16] XPREP, Version 5.1; Siemens Industrial Automation Inc., Madison, WI, 1995.
[17] G.M. Sheldrick, SHELXTL Reference Manual, Version 5.1; Bruker AXS, Madison, WI, 1997.
[18] G.M. Sheldrick, SHELXL-97: Program for Crystal Structure Refinement, University of Göttingen, Göttingen, Germany, 1997.
[19] M.A. Spackman, P.G. Byrom, Chem. Phys. Lett. 267 (1997) 215–220.
[20] J.J. McKinnon, M.A. Spackman, A.S. Mitchell, Acta Cryst. B60 (2004) 627–668.
[21] S.K. Wolff, D.J. Grimwood, J.J. McKinnon, D. Jayatilaka, M.A. Spackman, CrystalExplorer 2.0, University of Western Australia, Perth, Australia, 2007.
[22] F.H. Allen, O. Kennard, D.G. Watson, L. Brammer, A.G. Orpen, R.J. Taylor, Chem. Soc. Perkin Trans. 2 (1987) S1–S19.
[23] M.J. Frisch et al., Gaussian 03, Revision E.01, Gaussian Inc., Wallingford CT, 2004.
[24] E. Pidcock, Chem. Commun. 27 (2005) 3457–3459.
[25] N.M. O'Boyle, A.L. Tenderholt, K.M. Langner, J. Comput. Chem. 29 (2008) 839–845.
[26] B. Kosar, C. Albayrak, Spectrochim. Acta A 78 (2011) 160–167.
[27] G.U. Bublitz, S.G. Boxer, Annu. Rev. Phys. Chem. 48 (1997) 213–242.
[28] J.O. Verbal, L.P. Londono, J. Chem. Inf. Comput. Sci. 42 (2002) 1241–1246.
[29] T.V. Nguyen, D.W. Pratt, J. Chem. Phys. 124 (2006) 1216–1219.
[30] W. Kaminsky, J. Appl. Cryst. 38 (2005) 566–567.
[31] W. Kaminsky, J. Appl. Cryst. 40 (2007) 382–385.